Detection of the 267 GHz $J = 1$-0 Rotational Transition of PH_3 in Saturn with a New Fourier Transform Spectrometer

ERIC W. WEISSTEIN

Division of Geological and Planetary Sciences
California Institute of Technology 170-25, Pasadena, California 91125

AND

E. SERABYN

Division of Physics, Mathematics, and Astronomy
California Institute of Technology 320-47, Pasadena, California 91125

To appear in: Icarus
submitted: December 14, 1993
revised: March 28, 1994
accepted: April 13, 1994

Abstract

In recent observations with a Fourier transform spectrometer at the Caltech Submillimeter Observatory, we have detected the highly pressure-broadened (FWHM = 11.2 GHz) J = 1-0 rotational transition of PH_3 (phosphine) on Saturn. By modeling the Saturnian atmosphere with a radiative transfer code, we find that the observed line profile is consistent with a constant PH_3 mole fraction of 3.0 $\pm$ 1.0 ppm in the upper troposphere. A best-fit to the depth of the line implies a cutoff at high altitudes, with no PH_3 present at pressures $\lesssim$ 100 mbar. The observed line depth, combined with the lack of a detectable emission core, implies that a cutoff in the PH_3 abundance occurs at a pressure between 13 and 140 mbar. We did not detect PH_3 in Jupiter, nor any other molecular lines between 195 and 295 GHz (1.54 mm and 1.02 mm, respectively) in either Jupiter or Saturn.

1. Introduction

Because of the strength of its spectral lines, the PH_3 molecule provides a valuable probe of the upper atmospheres of Jupiter and Saturn. PH_3 is thermochemically stable at high temperatures (Atreya 1986) and is thought to be transported to observable levels from the deep atmospheres of Jupiter and Saturn by convection (Ridgeway *et al.* 1976, Larson *et al.* 1980). In the upper atmospheres of the Jovian planets, PH_3 is then rapidly depleted via photodissociation by solar UV photons (Strobel 1977, Kaye and Strobel 1984, Atreya 1986). Phosphorous compounds have been proposed as the chromophores in the atmospheres Jupiter and Saturn (Prinn and Lewis 1975), but Saturn's more subdued coloration relative to Jupiter—despite its larger PH_3 abundance (Atreya 1986)—and the lack of PH_3 enrichment in Jupiter's Great Red Spot (Kim and Owen 1983, Drossart *et al.* 1990, Griffith *et al.* 1992) call this assertion into question.

Infrared measurements have already provided estimates of the PH_3 abundances in Jupiter and Saturn (Larson *et al.* 1980, Drossart *et al.* 1982, Kunde *et al.* 1982, Courtin *et al.* 1984, Drossart *et al.* 1990, Noll and Larson 1990). However, infrared spectra of the giant planets are littered with thousands of overlapping ro-vibrational transitions, making comparison of infrared measurements with atmospheric models (Courtin *et al.* 1984, Noll *et al.* 1988, Noll *et al.* 1989, Noll *et al.* 1990, Noll and Larson 1990) difficult. Uncertainties in PH_3 line strengths at infrared frequencies also impose significant limitations on the retrieval of mixing ratios for other species (Noll and Larson 1990). The millimeter and submillimeter spectra of the giant planets, by comparison, contain relatively few spectral lines, which are consequently well separated. Because there is little confusion between the pure rotational lines at millimeter/submillimeter wavelengths, mixing ratios can be retrieved with relative ease. Far-infrared observations can detect energetic rotational transitions (Haas *et al.* 1985, 1986), but measurements at these wavelengths have thus far attained only low signal-to-noise ratios, limiting their utility.

The millimeter and submillimeter continua of the giant planets are produced by the far wings of NH_3 inversion lines (Poynter and Kakar 1975), the fundamental NH_3 J = 1-0 rotational transition at 572 GHz and its first few overtones, and transitions of collisionally induced dipoles in molecular hydrogen (Goodman 1969, Berge and Gulkis 1976). Various minor species, including CO, HCN, NH_3, and PH_3, also have millimeter/submillimeter rotational transitions (Lellouch *et al.* 1984, Bézard *et al.* 1986). The high pressures found in the thick atmospheres of the Jovian planets result in substantial collisional broadening of spectral lines, producing for each species a Lorentzian lineshape centered at the transition frequency ν_0 and given by the functional form

$$I(\nu) = \frac{S}{\pi} \frac{\alpha}{(\nu - \nu_0)^2 + \alpha^2}$$

(Townes and Schawlow 1975, pp. 338-339), where α is the half-width at half maximum intensity [HWHM] and S is the line strength. In the Jovian planets, the full-width at half maximum [FWHM] of collisionally broadened lines should reach several to $\sim$ 10 GHz. In order to detect these highly pressure-broadened lines, a spectrometer with wide frequency coverage is necessary. Heterodyne receivers and bolometers are the most commonly used detectors for millimeter and submillimeter observations. Heterodyne receivers provide very high spectral resolution, but only small bandpasses (typically $\leq$ 1 GHz), making them ill-suited to planetary continuum and pressure-broadened line observations. On the other hand, the filters typically used in conjunction with bolometer continuum observations (Hildebrand *et al.* 1985, Orton *et al.* 1986) have bandpasses which are much broader than planetary spectral lines, sharply limiting their utility in planetary spectroscopy. A moderate resolution spectrometer, which combines a large bandpass with a resolution intermediate to the two cases above, is therefore required.

2. The Instrument

In order to study the millimeter and submillimeter spectra of the giant planets at moderate resolution, we have built a rapid-scan Fourier transform spectrometer [FTS] for use at the Caltech Submillimeter Observatory [CSO]. The CSO is located on Mauna Kea, Hawaii, at an altitude of 13,200 feet above sea level. At this altitude, the observatory is above most of the water contained in the Earth's atmosphere, so observations at submillimeter wavelengths are possible in a number of atmospheric windows between 150 and 1000 GHz (2.0 and 0.3 mm, respectively). Figure 1 shows a model of the zenith atmospheric transmission at the CSO for 1 mm precipitable H_2O, a typical quantity under good observing conditions.

The FTS, an earlier version of which is described in Serabyn *et al.* (1991), is mounted at the Cassegrain focus of the 10.4 m CSO telescope. Fourier transform spectrometers (e.g., Connes 1961, Vanasse and Sakai 1967, Schnopper and Thompson 1974, Oepts 1976, Brault 1985) function by splitting incident radiation into two beams, allowing each beam to reflect off a separate mirror, and then recombining the reflected beams. By smoothly translating one mirror of the FTS, the optical path difference [OPD] between the beams is varied continuously, producing an interferogram which is the Fourier transform of the incident radiation's spectrum. The spectral resolution is determined by the maximum OPD of the interferometer, which gives $\approx$ 205 MHz for the 44 cm travel of our instrument.

Fourier transform spectrometers do not require cryogenic cooling, so our instrument is operated at ambient temperature. Only the detector (in these observations, the CSO facility bolometer) need be cooled. Inside the bolometer's cryogenic dewar, the incident radiation in the field of view is concentrated by a Winston cone (Welford and Winston 1989) into an integrating cavity, where it is detected by a liquid ^{3}He-cooled Si bolometer with noise equivalent power of $\sim 10^{-14}$ W Hz$^{-1/2}$. For these observations, we used a Winston cone with a 30″ field of view.

The spectrometer's bandpass is fixed by a liquid helium cooled metal-mesh filter (Whitcomb and Keene 1980, Holah 1982) in the bolometer dewar. For our observations, we used a low-pass filter with a 10% high-frequency cutoff of $\sim$ 340 GHz. The low-frequency cutoff near 180 GHz was introduced by the waveguide-like cutoff of the Winston cone concentrator. A plot of the interferometer's responsivity at two spectral resolutions is shown by the solid lines in Figure 2. After several tests, it was determined that the $\sim$ 6 GHz ripple evident at high spectral resolution arises from reflective standing waves in the Winston cone. Fortunately, because our instrument has a nearly linear response, the ripple can approximately be divided out of planetary spectra.

3. Observations

Observing Saturn with the FTS and the broadband filter shown in Figure 2 on December 7, 1992 (UT), we detected a very broad ($\sim$ 10 GHz) and deep ($\sim$ 30%) absorption feature which we identified as the first rotational transition of PH_3 at 266.945 GHz. Before our next observing run, we acquired a new 16 bit A/D, improved the instrument's optical alignment, and removed several sources of electrical interference. As a result, we were able to reduce systematic noise and greatly improve the data quality. Observations on July 11, 1993 confirmed the December detection (in fact, the depth and width of the two observations were the same to within experimental uncertainty) and provided the spectra we present here. The sub-Earth latitude on Saturn was 13.1° on July 11, resulting in an observing geometry illustrated in the inset to Figure 3a. The average zenith optical depth through the Earth's atmosphere at 225 GHz (as measured by an on-site water vapor radiometer) was $\tau = 0.12$ for the Saturn observations and, a few hours later, $\tau = 0.19$ for observations of Venus (our calibration source). Although we also observed Jupiter, we saw no evidence for a 267 GHz PH_3 line with absorption greater than $\sim$ 5%—the smallest detectable limit set by our noise and systematics on Jupiter. In the case of Jupiter, the limiting factor was the reflective standing waves present in the Winston cone (Figure 2).

In order to allow removal of instrumental and beam effects from our data, we observed Venus over the same airmass range as Saturn. Fortunately, on July 11, the angular diameter of Venus (17.6″) almost perfectly matched that of Saturn (18.3″ × 16.4″, for a geometric mean of 17.4″). This advantageous match in size allowed a direct division of the Saturn spectrum by that of Venus, obviating the need for detailed beam coupling measurements and calculations. Unfortunately, because of Jupiter's large size, beam coupling could not be removed from its spectrum in this manner.

4. Data Reduction

In the millimeter/submillimeter portion of the spectrum, the Earth's atmosphere emits strongly at frequencies corresponding to a number of H_2O, O_2, O_3, and $O^{18}O$ transitions (Waters 1974). In addition, the wings of the many far infrared H_2O lines produce an emission continuum (see Figure 1). In order to subtract this emission from our planetary spectra, we make use of the standard (On − Off) ÷ (Hot − Off) procedure (Penzias and Burrus 1973). To implement this technqiue, each pair of FTS scans (one scan in each direction of mirror motion) "on" the source is followed by a pair of scans "off" the source, on empty sky. Our "off" scans were taken offset 360″ in azimuth, far enough away so that the telescope beam was entirely off each planet, but still close enough to provide a sky measurement at similar atmospheric opacity. Since

on-source observations suffer from atmospheric attenuation, an additional measurement is taken of a "hot," i.e. ambient temperature, blackbody (in our case, a small sheet of Eccosorb) placed over the spectrometer's collecting mirror to provide an unattenuated blackbody spectrum.

In order to obtain planetary spectra from the individual "on," "off," and "hot" scans, we made use of the following equations of radiative transfer (derived in the Rayleigh-Jeans limit, where it is assumed that the Planck function is well-approximated by $B \propto T$; at these frequencies, this introduces an error no larger than 2%). In this approximation, the Earth's atmosphere is treated as an absorber/emitter with optical depth τ. The opacity of the Earth's atmosphere attenuates flux from astronomical sources by a factor $e^{-\tau}$, producing a transmitted brightness temperature $T_{\rm pla}e^{-\tau}$ for a source with disk-averaged brightness temperature $T_{\rm pla}$. In addition to attenuating the source flux, the Earth's atmosphere also emits. By Kirchhoff's Law, if the atmosphere were in equilibrium at temperature $T_{\rm sky}$, it would emit radiation in order to exactly balance the radiation it absorbed, giving an atmospheric radiation temperature of $T_{\rm atm} = T_{\rm sky}(1 - e^{-\tau})$. In practice, a sky efficiency $\eta_{\rm sky}$ must be inserted appropriately to account for the telescope's hot spillover (that fraction of the beam intercepted by ambient temperature surfaces—such as the feedlegs). In addition, because the telescope's beam becomes less responsive away from the pointing center, a frequency-dependent beam coupling efficiency $\eta_{\rm c}$ modifies the $T_{\rm pla}$ term (Ulich and Haas 1976, Kutner and Ulich 1981, Kutner *et al.* 1984). Finally, a temperature $T_{\rm port\ 2}$ must be subtracted to account for emission entering the interferometer from its second input port (Brault 1985) which, for our instrument, is reflected back to the detector. The equations describing our observations are therefore

$$V_{\rm on} = G[\eta_{\rm c}\eta_{\rm sky}T_{\rm pla}e^{-\tau} + \eta_{\rm sky}T_{\rm sky}(1 - e^{-\tau}) + (1 - \eta_{\rm sky})T_{\rm hot} - T_{\rm port\ 2}] \quad (1)$$

$$V_{\rm off} = G[\eta_{\rm sky}T_{\rm sky}(1 - e^{-\tau}) + (1 - \eta_{\rm sky})T_{\rm hot} - T_{\rm port\ 2}] \quad (2)$$

$$V_{\rm hot} = G[T_{\rm hot} - T_{\rm port\ 2}], \quad (3)$$

where V is the detected voltage, G is the instrumental gain, and all other terms are as defined above. Taking [(1)-(2)] ÷ [(3)-(2)] and rearranging gives

$$\eta_{\rm c}T_{\rm pla} = \left[\frac{V_{\rm on} - V_{\rm off}}{V_{\rm hot} - V_{\rm off}}\,T_{\rm sky}\right]\left[1 + e^{\tau}\left(\frac{T_{\rm hot}}{T_{\rm sky}} - 1\right)\right]. \quad (4)$$

If we now take $T_{\rm hot} \approx T_{\rm sky}$, this simplifies to

$$\eta_{\rm c}T_{\rm pla} = \frac{V_{\rm on} - V_{\rm off}}{V_{\rm hot} - V_{\rm off}}\,T_{\rm sky}, \quad (5)$$

so inserting the measured value of 273 K for $T_{\rm sky}$ then gives $\eta_{\rm c}T_{\rm pla}$.

The quantity obtained with the aid of (5) above, $\eta_{\rm c}T_{\rm pla}$, is the measured antenna temperature corrected for atmospheric extinction and hot spillover. This quantity is conventionally denoted T_A^* (Kutner and Ulich 1981). Since $T_{\rm pla} = T_A^*/\eta_{\rm c}$, T_A^* differs from the disk-averaged brightness temperature by the multiplicative factor $\eta_{\rm c}^{-1}$, so the beam coupling would normally have to be determined and removed. However, because the angular sizes of Venus and Saturn were so well matched during our observations, we were able to bypass the complications of beam coupling by simply dividing the two planetary spectra by each other, cancelling out the coupling efficiency in the process (this procedure works best if the Earth's atmospheric opacity is unchanged between the two planetary observations). An additional advantage of the division is its elimination of residual optical standing waves remaining in the spectra.

This division process does not account for Saturn's rings. It also ignores differences between telescope coupling to the projected ellipse of Saturn's disk and the projected circle of Venus's. However, we expect the effects of Saturn's rings and oblateness to be rather small ($\sim$ 10% and $<$ 1%, respectively) and therefore that the division provides a successful calibration to better than the 10% level. After division, the resultant spectrum was scaled to an absolute brightness temperature scale using a linear fit to published continuum brightness temperatures for Venus (see Table I) at 150, 230, and 300 GHz by Ulich (1981), Clancy and Muhleman (1991), and Werner *et al.* (1978).

The reduced spectra for Saturn, Venus, and Jupiter, in the standard units of T_A^* (equation 5), are shown in Figure 3. A residual ripple due to the multiple reflections in the Winston cone is present in all three

spectra, but the 267 GHz PH_3 line in Saturn stands out prominently. The 230 GHz CO line is also readily apparent on Venus, as can be seen in the inset to Figure 3b showing the Venus/Saturn ratio spectrum. Observations of CO in Venus will be discussed in a future publication. The instrumental uncertainty in frequency was estimated by fitting the narrow CO line in Venus. A fit to this line using an exponential lineshape and linear baseline yielded a central frequency of 230.543 GHz, compared to the actual frequency (in the absence of Doppler shift) of 230.538 GHz (Pickett *et al.* 1992). The surprisingly good agreement of 5 MHz is only 2% of a resolution element, demonstrating that instrumental frequency uncertainty is negligible.

Dividing the Saturn spectrum by that of Venus, and normalizing as discussed above, yields the final brightness temperature spectrum shown in Figure 4 (in which the region near the narrow Venusian CO line has been blanked). As can be seen in Figure 4, the division was successful in eliminating most of the residual instrumental ripple. Of other expected lines in Saturn (Bézard *et al.* 1986), the 216 GHz H_2S line is not apparent, nor is the 230 GHz CO line (Figure 3a) or the 266 GHz HCN line. Because of Jupiter's large size, beam coupling and instrumental ripples could not be removed using Venus as a calibrator. No spectral lines at all are evident in the the uncalibrated Jupiter spectrum.

4.1. Saturn Continuum Brightness Temperature

We first compare our derived Saturn continuum brightness temperatures to previously published measurements. In spite of the variations introduced by a ring geometry which differs among the published observations, the agreement of our derived continuum level with previous broad-band measurements is quite good. Fitting a linear slope to the continuum, we obtain a Saturnian brightness temperature of 139 K at 195 GHz (1.5 mm) and 148 K at 295 GHz (1.0 mm), consistent with the 137 ± 11 K Saturnian system brightness temperature reported by Ulich (1981) at 150 GHz and the 145 ± 7 K temperature quoted by Werner *et al.* (1978) at 300 GHz, but slightly larger than the 134.2 ± 3.2 K temperature given by Hildebrand *et al.* (1985) at 310 GHz. A summary of published brightness temperature measurements of the Saturnian system, including older values, is given in Table II.

There are a number of factors which could influence the continuum level and slope of our Saturn spectrum. The first, as already discussed, is the uncertainty present in the brightness temperature of Venus, the calibration source. In particular, the brightness temperature of Venus at 150 GHz (Ulich 1981) has an appreciable uncertainty and could potentially skew the slope used to convert the flux scale of Saturn to brightness temperature units. Secondly, the continuum level and slope are affected by the contribution of ring emission, which itself has a slight (but poorly determined) slope (Muhleman and Berge 1982). A third factor is the approximation of equation (4) by (5), combined with a possibly small difference between T_{sky} and T_{hot}. Finally, at this early stage of our instrumental development, we cannot rule out slight instrumental or weather-related effects. In light of these uncertainties, we adopt 144 K—the average measured continuum temperature—as our best estimate of Saturn's brightness temperature (including ring contributions) in the 195 to 295 GHz frequency range.

4.2. Saturn PH_3 Line Parameters

Since Doppler broadening is negligible (making consideration of a Voigt profile unnecessary), we first fit a Lorentzian lineshape with a linear baseline to the PH_3 line (Figure 4) using a nonlinear least squares algorithm. We fit the spectrum (1) allowing all parameters (line center, width, and depth; continuum average and slope) to vary, and (2) with the line center fixed at the PH_3 transition frequency (dashed curve in Figure 4). The two fits both gave a FWHM of 11.2 GHz, a line center depth of 48 K ($\sim$ 34% of the continuum, giving a brightness temperature at line center of $\sim$ 98 K), and an integrated area of 840 K GHz. When the line center frequency was allowed to vary, the solution converged to $\nu_0 = 267.5$ GHz. Because of the small resultant frequency offset from the true line center (< 5% of the line's FWHM and < 3 resolution elements) and accompanying agreement to better than 1% in both FWHM and depth between the two trials, the derived line parameters appear to be quite reliable.

5. Saturn Modeling

In order to determine the PH_3 mole fraction indicated by our data, we used a radiative transfer code to generate model spectra for various PH_3 mole fractions and cutoff pressures. The model, a modification of the code described in Grossman *et al.* (1989) and Grossman (1990), is discussed in some detail in the Appendix. In this model, ring absorption and emission are included to generate a disk averaged brightness temperature for Saturn and its rings. The disk averaged continuum brightness temperature predicted by

this Saturn model is 137 K at 200 GHz, falling slightly to 136 K at 295 GHz. These model temperatures are reasonably close to the measured $\sim$ 144 K temperature, although the continuum slope of the model (which is rather sensitive to the assumed frequency dependence of the ring brightness temperatures) is appreciably smaller than that measured. In addition to agreeing well with our observations, the model is also consistent with the predictions of other published Saturn models. In fact, when we suppress disk averaging and ring contributions to our model, we obtain brightness temperatures within several K of those predicted by the model of Lellouch *et al.* (1984) at our frequencies.

Potential uncertainties in our Saturn whole disk brightness temperature model include the assumed NH_3 mixing ratio, uncertainties in the pressure-temperature profile, and inaccuracies inherent in ring modeling. Because NH_3 is the primary opacity source in the continuum of Saturn near 200 GHz, the NH_3 distribution determines the continuum level. However, since tropospheric NH_3 is assumed to follow a saturation law down to the base of the NH_3 cloud, and because the atmospheric optical depth at frequencies between 195 and 295 GHz exceeds unity while still in the saturation region of NH_3 (Grossman 1990), varying the NH_3 mole fraction has a negligible effect on the model continuum brightness temperature. Similarly, despite variations in the atmospheric pressure-temperature profile of up to 10 K with latitude (Prinn *et al.* 1984, Lindal *et al.* 1985), the model brightness temperature is almost independent of the particular profile chosen. The explanation lies once again in the NH_3 saturation law, which allows the NH_3 cloud to move in altitude in response to a temperature offset to a new pressure which corresponds to the original temperature (Grossman 1990). Unlike the NH_3 mixing ratio and pressure-temperature profile, the nature of the model used to characterize emission and absorption by the rings is capable of producing appreciable ($\lesssim$ 10%) differences in whole disk model brightness temperatures. Fortunately, the simple ring model discussed in the Appendix appears to match our observations adequately.

5.1. HCN

Our whole disk models excluded the contribution from the HCN rotational transition at 265.886 GHz, near the PH_3 line center. Instead, because any HCN present in the stratosphere will appear in emission against the wings of the tropospheric PH_3, we used the lack of an HCN emission core in our spectrum to investigate an upper limit for the HCN mole fraction on Saturn. Figure 5 shows Saturn models generated assuming constant stratospheric HCN mole fractions (and no cutoff) of 2 ppb and 4 ppb. Because HCN has not yet been detected in Saturn, we used a simple constant mixing ratio model rather than the more detailed saturation law model of Bézard *et al.* (1986).

Considering the root-mean-square noise in Figure 4, we should have detected the HCN line if it had a resolution-convolved central height $> 3\sigma \approx 10.5$ K, corresponding to a mole fraction of 4 ppb (Figure 5). Therefore, the lack of an emission core in our data places an upper limit of $\sim$ 4 ppb on the HCN mole fraction in the stratosphere Saturn. This limit is smaller than the 8 ppb upper limit determined by Tokunaga *et al.* (1981). For such a small mole fraction, the modeled width of the HCN line is much narrower than that of PH_3. In fact, at 300 MHz from the HCN line center, the contribution from 4 ppb of HCN to the observed spectrum should already be negligible. Furthermore, the HCN abundance in the upper troposphere at pressures < 0.8 bar is limited by saturation and consequently is expected to be significantly smaller than 4 ppb (Bézard *et al.* 1986). Since the contribution from HCN should not appreciably affect the width of the very deep and wide PH_3 line, we disregarded HCN in subsequent modeling of the PH_3 line.

5.2. PH_3 Cutoff

We concentrate now on the distribution of PH_3 in the Saturnian atmosphere. Because PH_3 is destroyed by UV photolysis in the upper atmosphere, there is reason to believe that there exists some altitude above which all PH_3 is effectively destroyed. We call the pressure corresponding to this altitude the PH_3 cutoff pressure, p_c, and assume PH_3 is present only at pressures $p > p_c$. Since Saturn's atmosphere has a temperature inversion at $\sim$ 60 mbar, any PH_3 present at pressures less than 60 mbar would be seen as an emission spike at line center (superimposed on PH_3 absorption in the wings). No such emission core is observed in our data, so comparison with models generated for various cutoff pressures (Figure 6) indicates that, in order for the emission spike not to have been detectable ($\leq 3\sigma$), $p_c \gtrsim 13$ mbar. This result is consistent with the UV observations of Winkelstein *et al.* (1983), which imply an absence of PH_3 above the 25 mbar level.

5.3. PH_3 Mole Fraction

Finally, we discuss the actual pressure-broadened lineshape of PH_3. The high PH_3 absorption coefficient near line center makes Saturn's atmosphere highly opaque, so brightness temperature measurements near

line center probe the atmosphere at pressures only slightly greater than the true cutoff pressure (note that the value for p_c given above is a lower limit only). In the troposphere, the depth of the absorption becomes smaller as p_c (and the corresponding temperature) is increased. The observed central line depth is therefore a good indicator of the atmospheric cutoff level. Models with PH_3 cutoff pressures in the range 50-400 mbar were investigated (Figure 7). A cutoff pressure of 100 mbar was found to reproduce the observed line depth most accurately but, allowing for uncertainties in the data, models with p_c up to 140 mbar are capable of reproducing the observed line depth. For larger p_c, the predicted line depths are too small to agree with our measurements. Combining with the results of Section 5.2, we thus find 13 mbar $< p_c <$ 140 mbar.

Using our best value of p_c = 100 mbar, we ran models for a suite of PH_3 mole fractions, each assumed to be constant at pressures $p > p_c$. PH_3 is expected to undergo rapid depletion with altitude, resulting in a depletion scale height of $\sim$ 3.5 km for an eddy diffusion coefficient of $K \sim 10^4$ cm^2s^{-1} (Kaye and Strobel 1984). Since the depletion scale height is small compared to the pressure scale height of $\sim$ 40 km, the simplest PH_3 model, consisting of a constant mixing ratio below the cutoff pressure ($\sim$ pressure of peak photodissociation), is expected to provide an adequate fit to our observations. In light of the slight continuum slope difference betwen our nominal model and observations, we removed linear baselines from the disk average brightness temperatures generated by our model and reinserted baselines matching the measured Saturn spectrum.

As revealed by Figure 8, which shows model curves for three PH_3 mole fractions superimposed on the Saturn spectrum, the observed *linewidth* is quite sensitive to the abundance of PH_3 because of opacity in the line wings. The observed PH_3 linewidth therefore provides a robust indicator of PH_3 mole fraction. By performing chi-squared tests of the fits, we obtained a best-fit PH_3 mole fraction of 3.0 ppm (see Table III). Based on the sensitivity of the fit to the model mole fraction, we estimate the uncertainty in our PH_3 determination to be $\sim \pm 1.0$ ppm.

5.4. PH_3 Temperature Broadening Exponent

Because the temperature line-broadening exponent for the 267 GHz PH_3 transition has not been measured in the laboratory, our models assumed the same exponent as for NH_3 (Berge and Gulkis 1976), $n = 0.67$, where n is defined by $\Delta\nu \propto (T_0/T)^n$, $\Delta\nu$ is the line width, and T_0 is a reference temperature. We also investigated models using values of n ranging from 0.5 to 1.0 because $n = 0.5$ corresponds to "hard" collisions (Townes and Schawlow 1975, p. 368), and experimental temperature exponents for microwave transitions of molecules possessing typical intermolecular forces commonly lie in the range 0.7-1.0 (Waters 1974). The change in linewidth obtained by varying n in our model yielded PH_3 mixing ratio retrievals which differed from our nominal 3.0 ppm by $\pm$ 0.3 ppm, much less than our estimated uncertainty of $\pm$ 1.0 ppm (see Table IV) and negligible when combined with it in quadrature. Therefore, our determination of the PH_3 mole fraction in Saturn is rather insensitive to the precise numerical value of n.

5.5. Weighting Functions

With a PH_3 mole fraction of 3.0 ppm, the pressures at which PH_3 absorption occurs are illustrated in the weighting function plots shown in Figure 9. In the continuum ($\Delta\nu = 10\alpha$; Figure 9a), almost all emission comes from NH_3 inversion line wings at a pressure of $\sim$ 1.4 bar. Near the PH_3 line center, on the other hand, the line originates from higher up, as a result of the large PH_3 opacity. Very close to line center at $\Delta\nu = 0.5\alpha$ (Figure 9d), the weighting function peaks at roughly 150 mbar, but at one half width away from line center at $\Delta\nu = \alpha$ (Figure 9c), we see to several hundred mbar. At $\Delta\nu = 1.5\alpha$ (Figure 9b), the PH_3 weighting function is decreasing in strengh and moving downward, so the contribution from NH_3 dominates the weighting function (although PH_3 contributes down to $\sim$ 1 bar). The predominant contributions to PH_3 opacity therefore arise from pressures of $\sim$ 100-1000 mbar, varying across the line profile. Because all these contributions to Saturn's opacity arise above the cloud decks (which form at pressures > 1.4 bar), we need not consider the effects of clouds.

6. Jupiter Modeling

Because of Jupiter's large size ($35.2'' \times 33.0''$) during our July observations, beam coupling effects could not be removed solely using Venus as a calibrator. Since both Jupiter and the Moon filled our 30″ field of view, we attempted to use the Moon as a calibration source. Unfortunately, this technique did not satisfactorily remove the instrumental ripple. A better characterization of the beam coupling, to be undertaken in future

observations, is therefore needed before we are able to convert the Jupiter spectrum shown in Figure 3c from T_A^* units to absolute brightness temperatures.

Despite this shortcoming, it is still possible to place a rough upper limit on the PH_3 mole fraction in Jupiter. The measured continuum brightness temperature of Jupiter at relevant millimeter wavelengths is given by various authors as 158 ± 10 K (Courtin *et al.* 1977) and 166-175 K (Joiner *et al.* 1992) at 214-215 GHz, and 165 ± 8 K (Ulich *et al.* 1984) and 169-197 K (Joiner *et al.* 1992) at 227-230 GHz. [A tabular summary of Jupiter millimeter wave observations is presented in Joiner and Steffes (1990).] Assuming that a PH_3 absorption line could be detected if it had depth roughly half the size of the peak-to-peak ripple amplitude in Figure 3c, scaling Figure 3c to the temperature of Ulich *et al.* (1984) then implies a brightness temperature limit of 15 K for the PH_3 line in Jupiter.

To estimate the phosphine abundance required to produce such a line depth, we modeled Jupiter's atmosphere in a similar manner to that discussed for Saturn. We assumed a constant PH_3 mixing ratio with no photochemical cutoff, used H_2, He, and CH_4 mole fractions of 0.895, 0.102, and 0.003, respectively, and assumed a sub-cloud NH_3 mole fraction of 2.6×10^{-4}. These values were obtained by rescaling the least-squares fits from various observations given by Fegley (1992) to obtain a sum of unity. Our models indicated that a PH_3 mole fraction of 0.5 ppm would yield a line depth of $\sim$ 15 K and a FWHM of $\sim$ 1.6 GHz. The absence of a PH_3 line in our observations therefore implies an upper limit for PH_3 in Jupiter of $\sim$ 0.5 ppm (assuming a constant mixing ratio). This upper limit is consistent with the observed PH_3 mixing ratios of 0.09-0.18 ppm ($\leq$ 560 mbar), 0.35 ppm (500 mbar), and 0.30 ppm (600 mbar) determined from 10 μm infrared spectroscopy by Tokunaga *et al.* (1979), Kunde *et al.* (1982), and Griffith *et al.* (1992). The slightly higher mole fraction of 0.54 ppm reported by Larson *et al.* (1977) is derived from 5 μm spectroscopy, and therefore corresponds to deeper atmospheric levels than those sensed by millimeter observations. Because our rough PH_3 estimate is greatly limited by presence of ripples in our data, it remains possible that reducing the size of the instrumental ripple would allow detection PH_3 in Jupiter in future observations.

7. Interpretation

A summary of Saturnian PH_3 abundances inferred by various observers is given in Table V. Most infrared observations of Saturn prior to 1984 were at wavelengths of 3 and 10 μm. These observations sampled the Saturnian atmosphere at pressures of $P \sim$ 400-700 mbar and obtained PH_3 abundances between 0.8 and 2.0 ppm (summarized in Prinn *et al.* 1984). However, measurements by Bézard *et al.* (1987) at 5 μm—a more transparent region of the spectrum—suggested that the PH_3 concentration was significantly higher at the $\sim$ 4 bar level. Similarly, Noll and Larson (1990) reported a best fit to 3 and 10 μm infrared observations—taking into account evidence for higher abundances at the pressures sampled by 5 μm measurements—with a PH_3 mole fraction of 1 ppm for 78 mbar $< p <$ 400 mbar and 7^{+3}_{-2} ppm for $p >$ 400 mbar (where the transition pressure is that of the upper cloud in their two-cloud model). However, the model of Noll and Larson was not optimized for the upper troposphere (i.e., that portion of the atmosphere above the base of the NH_3 clouds at pressures $\leq$ 1.4 bar).

Infrared observations suffer from a lack of prominent PH_3 features, making it difficult to isolate PH_3 emission from that due to other continuum sources. An exception is the 1972 cm^{-1} Q-branch observed at 5 μm in Saturn by Bézard *et al.* (1987). Comparison with the laboratory measurements of Tarrago *et al.* (1992) allowed these authors to derive a PH_3 mole fraction of $\sim$ 5 ppm in the deep Saturnian atmosphere. However, the analysis of 5 μm observations of Saturn is complicated by their sensitivity to reflected solar flux from a few hundred millibars in addition to thermal radiation from several bars. Noll and Larson used micro-windows in the 2000-2160 cm^{-1} region to determine the 7 ppm lower tropospheric PH_3 mole fraction for their model. Although Noll and Larson were able to fit portions of their spectrum (which contains nearly 2000 PH_3 lines) quite well, they had difficulty matching the entire spectrum, possibly as a result of the discontinuous vertical mole fraction profile they used. Finally, infrared abundance inversions are sensitive to assumptions about cloud heights and structure. All these factors conspire to make an unambiguous estimate of the true PH_3 mixing ratio from infrared measurements very difficult, although these measurements do give convincing evidence for a drop in PH_3 abundace with increasing altitude.

Millimeter measurements avoid the complications inherent in infrared work because they are sensitive only to thermal emission from the upper troposphere (pressures $<$ 1.4 bar; see Figure 9) and are unaffected by reflected solar flux (which is negligible at millimeter wavelengths). The presumed "upper cloud" at 400

mbar (Tomasko *et al.* 1984) can also be ignored since its opacity is negligible at wavelengths longer than infrared. The constant PH_3 mole fraction of 3.0 ± 1.0 ppm which we derive is intermediate to the 3/10 μm and 5 μm-derived values discussed above. However, this is not due to our sampling of pressures intermediate to the two IR bands, since the central portion of the 267 GHz PH_3 line arises from higher in the atmosphere than do the IR lines. As a result, our measurements imply a PH_3 mole fraction in the upper troposphere of Saturn which is considerably larger than the previously published values.

In order to make a more direct comparison of our observations with the two-step PH_3 abundance profile derived by Noll and Larson (1990), we also ran atmospheric models using the profile suggested by these authors. We found that a mole fraction of 1 ppm for 78 mbar $< p <$ 400 mbar and 7 ppm for $p >$ 400 mbar resulted in a PH_3 line width somewhat too narrow and a line depth too small to be consistent with our observations (Figure 10), as confirmed by a chi-squared test (see Table III). However, the difference from our best one-step model is not large. It should in principle be possible to model the PH_3 line with various abundance profiles and to use chi-squared testing to determine the profile matching our observations most closely. For example, we could use more complicated exponential profiles such as those adopted by Tokunaga *et al.* (1979), Tokunaga *et al.* (1980), Haas *et al.* (1985), or Griffith *et al.* (1992). Unfortunately, although the central portion of the observed PH_3 absorption line can be fit fairly cleanly, the remnant ripple evident in Figure 4 would make it difficult to distinguish small differences in the wing lineshape, implying that our data do not yet warrant a parameterization beyond the first-order one-step approximation. The simple one-step PH_3 model we use is already consistent with a convective origin for tropospheric PH_3 in Saturn, since convection should result in a well-mixed, nearly constant tropospheric PH_3 mixing ratio up to the level at which PH_3 is most effectively destroyed by photodissociation, making it adequate for our analysis. Further improvements in the spectrometer, as well as a measurement of the J = 3-2 line near 800 GHz, should eventually provide data of sufficiently high quality to warrant more detailed modeling.

Finally, we address the question of time dependence. The "Great White Spot" equatorial atmospheric disturbance that occurred in Saturn in late September of 1990 (Westphal *et al.* 1992) may have resulted in an increase in the transport of PH_3 to the atmospheric levels at which we observed it. Because we have no data prior to December 1992, we are unable to compare observations before and after the event in order to address this possibility. However, no change occurred in the millimeter spectrum of Saturn between December 1992 and July 1993.

8. Conclusions

The non-detection of a narrow stratospheric emission core at the line center of the J = 1-0 PH_3 rotational transition in Saturn provides a lower limit on the PH_3 cutoff pressure in Saturn's stratosphere of at least 13 mbar, consistent with a low stratospheric PH_3 mixing ratio. The depth of the absorption line also places an upper limit of 140 mbar on the PH_3 cutoff pressure, with 100 mbar providing the best fit to our observations. By comparing the width of the observed PH_3 transition in Saturn with that modeled for various abundances, we obtain an estimate of the Saturnian PH_3 mole fraction of 3.0 ± 1.0 ppm in the pressure range from $\sim$ 1 bar to 100 mbar (assuming a constant mole fraction at pressures greater than the $\sim$ 100 mbar cutoff pressure). This abundance represents an enrichment of more than 5 times the solar value of $(P/H)_\odot = 2.7 \times 10^{-7}$ (Anders and Grevesse 1989) and is larger than the Saturnian PH_3 abundance derived from previous infrared measurements at these pressures. Our observations of Jupiter indicate that the PH_3 abundance is depleted by at least a factor of 7 over that in Saturn. While this depletion might be partially explained by Jupiter's greater gas retention during its formation, it seems likely that other factors, such as the convective transport rate from the deep atmosphere, may play a role.

Our ability to probe the PH_3 mixing ratio as a function of altitude is currently limited both by the fact that we have thus far observed only the fundamental J = 1-0 transition, and by systematic instrumental effects. It should be possible to refine our measurements in the near future by observing the J = 3-2 rotational lines of PH_3 near 800 GHz, and by making further improvements to the FTS. We also plan to apply more robust calibration techniques involving full beam coupling measurements to allow more accurate determinations of brightness temperatures.

Moderate resolution FTS observations of the planets in the millimeter/submillimeter region show great potential for furthering our understanding of molecular abundances and distributions in planetary atmospheres. In particular, as we explore higher frequencies, we hope to detect and model other species (such as

CO, HCN, NH_3, and H_2S) in the atmospheres of the Jovian planets. FTS observations in this portion of the spectrum can also measure planetary continuum temperatures over much wider bandpasses than previously possible. The results presented in this paper are therefore only the first of what we anticipate to be many interesting new results in wide-band millimeter/submillimeter planetary spectroscopy.

Appendix: Radiative Transfer Model

The radiative transfer model used to calculate the synthetic spectra presented in this paper is based on the code of Grossman *et al.* (1989) and Grossman (1990), which in turn is a synthesis of the classic review paper of Berge and Gulkis (1976) and previous modeling work by Atreya and Romani (1985) and de Pater and Massie (1985). At pressures smaller than 1.4 bar on Saturn, the model uses the pressure-temperature profile derived by Lindal *et al.* (1985) and Lindal (1992) from the Voyager 2 ingress radio occultation. In order to ensure that the opacity remains reasonably small in each layer, the pressure-temperature profile of Lindal is interpolated to smaller logarithmically spaced layers. Temperature is then adiabatically extrapolated downward to pressures of several bars (Figure 11). A wet adiabat is used for the extrapolation (Atreya and Romani 1985). At present, the "frozen" value for the heat capacity of hydrogen (Massie and Hunten 1982) is adopted.

The opacity sources included in the model are emission from H_2 dipoles induced by H_2-He and H_2-H_2 collisions, NH_3 inversion lines, the three NH_3 rotational lines at 572.4, 1168.5, and 1215.2 GHz, and the 11 PH_3 rotational lines with frequencies less than 1200 GHz and integrated intensities at 300 K greater than 10^{-7} nm^2MHz. In addition, the 21 HCN lines with frequencies less than 1250 GHz and the 11 CO lines with frequencies less than 1300 GHz are included in the code. However, because our measurements did not detect CO or HCN, and because the mole fractions of these species in Saturn are not well known, CO and HCN were not included in the models which we compared to our observed spectra. The frequencies, line strengths, and energies for NH_3, PH_3, HCN, and CO lines were taken from Pickett *et al.* (1992). Mole fractions of H_2, He and CH_4 in Saturn were taken to be 96.30%, 3.25%, and 0.45%. These represent the best values obtained by Voyager IRIS measurements (Conrath *et al.* 1984, Courtin *et al.* 1984). NH_3 is assumed to follow a saturation law above the NH_3 cloud, and the unsaturated mole fraction of NH_3 is taken as the solar value of 1.7×10^{-4} (Atreya 1986).

The opacity contributed by spontaneous dipole formation induced by the collisions of H_2-He and H_2-H_2 is parameterized using the formalism of Goodman (1969), discussed in Berge and Gulkis (1976). Goodman's equation extrapolates the values computed by Trafton (1965) and gives opacity as a function of temperature and H_2 and He partial pressures. The 119 NH_3 inversion lines with wavelengths longer than 1.3 cm (Poynter and Kakar 1975, Pickett *et al.* 1992) are summed over using a Van Vleck-Weisskopf lineshape (Townes and Schachlow 1975). A Ben Reuven (Waters 1974) lineshape has been found to best-fit observations at frequencies less than 30 GHz, but the Van Vleck-Weisskopf line shape appears to provide a better fit at higher frequencies (Berge and Gulkis 1976, de Pater and Massie 1985). Recent measurements, however, indicate that both the Van Vleck-Weisskopf and Ben Reuven lineshapes may provide an inadequate description of observations at centimeter and shorter wavelengths (Spilker 1993). Unfortunately, a new NH_3 lineshape formalism developed by Spilker is currently applicable only to frequencies less than $\sim$ 50 GHz (T. R. Spilker, pers. comm.). An alternate formalism, not used here, has been developed by Joiner and Steffes (1990).

The NH_3 rotational lines are assumed to have a Van Vleck-Weisskopf lineshape. The relevant functional form for each of these lines is taken from de Pater and Massie (1985). The rotational lines of all other species are modeled with a Lorentzian lineshape. The pressure broadening coefficients for the 266.945 GHz rotational transition of PH_3 in He and H_2 are taken from the room temperature laboratory measurements of Pickett *et al.* (1981). Because the temperature broadening exponent for this transition has not been measured, we used Pickett *et al.*'s measurements at 25° C and investigated exponents in the range 0.5-1.0 (see Section 5.4).

To compute whole disk models, the projection of a spheroidal Saturn to yield an elliptical "disk" is performed, and each grid point lying in the ellipse is converted to the corresponding latitude and longitude. After 1-D brightness temperatures are computed at each grid point, they are averaged together and expressed as an equivalent disk brightness temperature. The sampling grid size is chosen to be 0.5″ for Saturn, since nearly identical antenna temperatures were obtained in several trials using finer grid spacings.

The geometry of the A, B, and C rings and Cassini Division is fully accounted for in the Saturn model.

Attenuation of Saturn's flux by the ring cusps and thermal emission from the ring ansae are modeled using ring "brightness" temperatures and optical depths. Because the thermal emission of the rings increases appreciably with frequency in the millimeter/submillimter portion of the spectrum (Esposito *et al.* 1984), a linear slope in frequency was fit to the brightness temperatures of the combined A and B rings measured between 90 and 300 GHz by Epstein *et al.* (1984), Muhleman and Berge (1982), Dowling *et al.* (1987), Ulich (1974), Grossman (1990), and Werner *et al.* (1978). The slope was then used to extrapolate the brightness temperatures dervied for the individual rings by Grossman (1990, p. 52) at 150 GHz to nearby frequencies.

The optical depth of the combined A+B+C rings is observed to be independent of wavelength from the UV to a wavelength of 6 cm (Dowling *et al.* 1987). While the optical depths of the individual rings is not expected to be wavelength independent, not many values have been published for millimeter wavelengths. We therefore ran models using optical depths given by Grossman (1990, p. 59) at 2.01 cm and 6.17 cm. Optical depths at these two frequencies are similar for all rings except the A ring, where the 2.01 cm value given by Grossman appears to be anomalously high. Models generated using the two sets of optical depths gave similar results, with the 6.17 cm values yielding whole disk brightness temperatures ~ 3 K warmer. In subsequent modeling, we used the 6.17 cm ring optical depths given by Grossman, ignoring any frequency dependence.

Acknowledgments

We thank Vernon Overby of MXM, Inc. and Walt Schaal of Caltech for their assistance in cajoling the translation stage to move with the requisite smoothness and accuracy. We express our gratitude to the CSO staff—and particularly Antony Schinkel and Ken Young—for their assistance in coaxing all the pieces of our FTS to converse amicably with each other. We also thank Arie Grossman for providing the original atmospheric model on which our code is based, and for his informative thesis. Mark Gurwell and Duane Muhleman provided much useful input through illuminating discussions. In addition, we extend our thanks to Drs. Bruno Bézard and Keith Noll for their careful reading of the manuscript which led to many helpful suggestions and numerous clarifications. This work was supported by NSF grant AST-9313929 to the CSO and by NASA grants NAGW-3303 and NAGW-1448.

References

ANDERS, E. AND N. GREVESSE. 1989. Abundances of the elements: Meteoritic and solar. *Geochim. Cosmochim. Acta* **53**, 197-214.

ATREYA, S. K. 1986. *Atmospheres and Ionospheres of the Outer Planets and their Satellites.* Sec. 5.3: Phosphine (PH_3). Springer-Verlag, Berlin.

ATREYA, S. K. AND P. N. ROMANI. 1985. Photochemistry and clouds of Jupiter, Saturn, and Uranus. In *Recent Advances in Planetary Meteorology* (G. E. Hunt, Ed.), pp. 17-68. Cambridge Univ. Press, Cambridge.

BERGE, G. L. AND S. GULKIS. 1976. Earth-based radio observations of Jupiter: Millimeter to meter wavelengths. In *Jupiter* (T. Gehrels, Ed.), pp. 621-692. Univ. of Arizona Press, Tucson.

BÉZARD, B. 1985. Thermal structure of Saturn's atmosphere. In *The Atmospheres of Saturn and Titan* (E. Rolfe and B. Battrick, Eds.). ESA SP-241. European Space Agency, Paris.

BÉZARD, B., D. GAUTIER, AND A. MARTEN. 1986. Detectability of HD and non-equilibrium species in the upper atmospheres of the giant planets from their submillimeter spectra. *Astron. Astrophys.* **161**, 387-402.

BÉZARD, B., P. DROSSART, J. P. MAILLARD, G. TARRAGO, N. LACOME, G. POUSSIGUE, A. LEVY, AND G. GUELACHVILLI. 1987. High resolution spectroscopy of Saturn at 5 μm. II. Cloud structure and gaseous composition. *Bull. Amer. Astron. Soc.* **19**, 849.

BRAULT, JAMES W. 1985. Fourier Transform Spectroscopy. In *High Resolution in Astronomy: 15th Advanced Course of the Swiss Society of Astronomy and Astrophysics* (A. Benz, M. Huber, and M. Mayor, Eds.). Geneva Observatory, Sauverny, Switzerland.

BREGMAN, J. D., D. F. LESTER, AND D. M. RANK. 1975. Observation of the ν_2 band of PH_3 in the astmosphere of Saturn. *Astrophys. J.* **202**, L55-L56.

CLANCY, R. T. AND D. O. MUHLEMAN. 1985. Chemical-dynamical models of the Venus mesosphere based upon diurnal microwave CO variations. *Icarus* **64**, 183-204.

CLANCY, R. T. AND D. O. MUHLEMAN. 1991. Long-term (1979-1990) changes in the thermal, dynamical, and compositional structure of the Venus mesosphere as inferred from microwave spectral line observations of ^{12}CO, ^{13}CO, and $C^{18}O$. *Icarus* **89**, 129-146.

CONNES, J. 1961. *Rev. Opt.* **40**, pp. 45, 116, 171, 231. Available in English translation as NAVWEPS Report No. 8099, NOTS TP3157, U.S. Naval Ordnance Test Station, China Lake, Calif.

CONRATH, B. J., D. GAUTIER, R. A. HANEL, AND J. S. HORNSTEIN. 1984. The helium abundance of Saturn from Voyager measurements. *Astrophys. J.* **282**, 807-815.

COURTIN, R., N. CORON, T. ENCRENAZ, R. GISPERT, P. BRUSTON, J. LEBLANC, G. DAMBIER, AND A. VIDAL-MADJAR. 1977. Observations of giant planets at 1.4 mm and consequences on the effective temperatures. *Astron. Astrophys.* **60**, 115-123.

COURTIN, R., D. GAUTIER, A. MARTEN, B. BÉZARD, AND R. HANEL. 1984. The composition of Saturn's atmosphere at northern temperate latitudes from Voyager IRIS spectra: NH_3, PH_3, C_2H_2, C_2H_6, CH_3D, CH_4, and the Saturnian D/H ratio. *Astrophys. J.* **287**, 899-916.

DE PATER, I. AND S. MASSIE. 1985. Models of the millimeter-centimeter spectra of the giant planets. *Icarus* **62**, 143-171.

DOWLING, T. E., D. O. MUHLEMAN, AND G. L. BERGE. 1987. Aperture synthesis observations of Saturn and its rings at 2.7-mm wavelength. *Icarus* **70**, 506-516.

DROSSART, P., T. ENCRENAZ, V. KUNDE, R. HANEL, AND M. COMBES. 1982. An estimate of the PH_3, CH_3D, and GeH_4 abundances on Jupiter from the Voyager IRIS data at 4.5 μm. *Icarus* **49**, 416-426.

DROSSART, P., E. LELLOUCH, B. BÉZARD, J. P. MAILLARD AND G. TARRAGO. 1990. Jupiter–Evidence for a phosphine enhancement at high northern latitudes. *Icarus* **83**, 248-253.

EPSTEIN, E. E., M. A. JANSSEN, AND J. N. CUZZI. 1984. Saturn's rings: 3-mm low-inclination observations and derived properties. *Icarus* **58**, 403-411.

ESPOSITO, L. W., J. N. CUZZI, J. B. HOLBERG, E. A. MAROUF, G. L. TYLER, AND C. C. PORCO. 1984. Saturn's rings: Structures, dynamics, and particle properties. In *Saturn* (T. Gehrels, Ed.), pp. 463-545. Univ. of Arizona Press, Tucson.

FEGLEY, B. 1992 preprint. Properties and composition of the terrestrial oceans and of the atmospheres of the Earth and other planets. Submitted to *AGU Handbook of Physical Constants.*

GILLET, F. C. AND W. J. FORREST. 1974. The 7.5 to 13.5 micron spectrum of Saturn. *Astrophys. J.* **187**, L37-L38.

GOODMAN, G.C. 1969. Models of Jupiter's atmosphere. Ph.D. thesis. Univ. of Illinois, Urbana, Ill.

GRIFFITH, C., B. BÉZARD, T. OWEN, AND D. GAUTIER. 1992. The tropospheric abundances of NH_3 and PH_3 in Jupiter's Great Red Spot, from Voyager IRIS observations. *Icarus* **98**, 82-93.

GROSSMAN, A. W., D. O. MUHLEMAN, AND G. L. BERGE. 1989. High-resolution microwave images of Saturn. *Science* **245**, 1211-1215.

GROSSMAN, A. W. 1990. Microwave Imaging of Saturn's Deep Atmosphere and Rings. Ph.D. thesis. California Institute of Technology, Pasadena, Calif.

GROSSMAN, E. 1989. AT, atmospheric transmission software. Airhead Software, Boulder, Colo.

HAAS, M. R., E. F. ERICKSON, D. GOORVITCH, D. D. MCKIBBIN, AND D. M. RANK. 1985. Observations of the $J = 10$ manifold of the pure rotation band of phosphine on Saturn. *Icarus* **64**, 549-556, 1985.

HAAS, M. R., E. F. ERICKSON, D. GOORVITCH, D. D. MCKIBBIN, AND D. M. RANK. 1986. Erratum to: Observations of the $J = 10$ manifold of the pure rotation band of phosphine on Saturn. *Icarus* **67**, 342.

HANEL, R. A., B. J. CONRATH, F. M. FLASAR, V. G. KUNDE, W. MAGUIRE, J. C. PEARL, J. A. PIRRAGLIA, R. SAMUELSON, L. HEARTH, M. ALLISON, D. P. CRUIKSHANK, D. GAUTIER, P. GIERASCH, L. HORN, R. KOPPANY, AND C. PONNAMPERUMA. 1981. Infrared observations of the Saturnian system from Voyager 1. *Science* **212**, 192-200.

HILDEBRAND, R., R. LOWENSTEIN, D. HARPER, G. ORTON, J. KEENE, AND S. WHITCOMB. 1985. Far-infrared and submillimeter brightness temperatures of the giant planets. *Icarus* **64**, 64-87.

HOLAH, G. D. 1982. Far-infrared and submillimeter-wavelength filters. Ch. 6 in *Infrared and Millimeter Waves* **6**. Academic Press, New York.

JOINER, J. AND P. S. STEFFES. 1990. Modelling of the millimeter-wave emission of Jupiter utilizing laboratory measurements of ammonia opacity. *J. Geophys. Res.* **96**, 17462-17470.

JOINER, J., P. S. STEFFES, AND K. S. NOLL. 1992. Search for sulfur (H_2S) on Jupiter at millimeter wavelengths. *IEEE Trans. Microwave Theory Tech.* **40**, 1101-1109.

KAYE, J. A. AND D. F. STROBEL. 1984. Phosphine photochemistry in the atmosphere of Saturn. *Icarus* **59**, 314-335.

KIM, S. J. AND T. OWEN. 1983. PH_3 mixing ratio in the Great Red Spot. *Bull. Amer. Astron. Soc.* **15**, 832.

KUNDE, V., R. HANEL, W. MAGUIRE, D. GAUTIER, J. BALUTEAU, A. MARTEN, A. CHÉDIN, N. HUSSON, AND N. SCOTT. 1982. The tropospheric composition of Jupiter's north equatorial belt (NH_3, PH_3, CH_3D, GeH_4, and H_2O) and the Jovian D/H isotopic ratio. *Astrophys. J.* **263**, 443-467.

KUTNER, M. L. AND B. L. ULICH. 1981. Recommendations for calibration of millimeter-wavelength spectral line data. *Astrophys. J.* **250**, 341-348.

KUTNER, M. L., L. MUNDY, AND R. J. HOWARD 1984. Interpretation of absolute line intensities on the NRAO 11 meter and other millimeter wave telescopes. *Astrophys. J.* **283**, 890-894.

LARSON, H. P., U. FINK, AND R. R. TREFFERS. 1977. Phosphine in Jupiter's atmosphere: The evidence from high-altitude observations at 5 micrometers. *Astrophys. J.* **211**, 972-979.

LARSON, H. P., U. FINK, H. A. SMITH, AND D. S. DAVIS. 1980. The middle-infrared spectrum of Saturn: Evidence for phosphine and upper limits to other trace atmospheric constituents. *Astrophys. J.* **240**, 327-337.

LELLOUCH, E., T. ENCRENAZ, AND M. COMBES. 1984. The detectability of minor atmospheric species in the far infrared spectra of Jupiter and Saturn. *Astron. Astrophys.* **140**, 405-413.

LINDAL, G. F., D. N. SWEETNAM, AND V. R. ESHLEMAN. 1985. The atmosphere of Saturn: An analysis of the Voyager radio occultation measurements. *Astron. J.* **90**, 1136-1146.

LINDAL, G. F. 1992. The atmosphere of Neptune: An analysis of radio occultation data acquired with Voyager 2. *Astron. J.* **103**, 967-982.

MASSIE, S. T. AND D. M. HUNTEN. 1982. Conversion of *para* and *ortho* hydrogen in the Jovian planets. *Icarus* **49**, 213-226.

MUHLEMAN, D. O. AND G. L. BERGE. 1982. Microwave emission from Saturn's rings. In *Planetary Rings* (A. Brahic, Ed.), pp. 57-70. I.A.U., Cepadues-Editions, Toulouse, France.

NOLL, K. S. 1987. Carbon monoxide and disequlibrium dynamics in Saturn and Jupiter. Ph.D. thesis, State Univ. of New York at Stony Brook.

NOLL, K. S., R. F. KNACKE, T. R. GEBALLE, AND A. T. TOKUNAGA. 1988. Evidence for germane in Saturn. *Icarus* **75**, 409-422.

NOLL, K. S., T. R. GEBALLE, AND R. F. KNACKE. 1989. Arsine in Saturn and Jupiter. *Astrophys. J.* **338**, 71-74.

NOLL, K. S., H. D. LARSON, AND T. R. GEBALLE. 1990. The abundance of AsH_3 in Saturn. *Icarus* **83**, 494-499.

NOLL, K. S. AND H. P. LARSON. 1990. The spectrum of Saturn from 1990 to 2230 cm^{-1}: Abundances of AsH_3, CH_3D, CO, GeH_4, NH_3, and PH_3. *Icarus* **89**, 168-189.

OEPTS, D. 1976. Fourier Transform Spectroscopy. In *Methods of Experimental Physics* **13**, Part B (Spectroscopy) (Dudley Williams, Ed.), pp. 60-87. Academic Press, New York.

ORTON, G., M. GRIFFEN, P. ADE, I. NOLT, J. RADOSTITZ, E. ROBSON, AND W. GEAR. 1986. Submillimeter and millimeter observations of Uranus and Neptune. *Icarus* **67**, 289-304.

PENZIAS, A. A. AND C. A. BURRUS. 1973. Millimeter-wavelength radio-astronomy techniques. *Ann. Rev. Astron. Astrophys.* **11**, 51-72.

PICKETT, H.M., R. L. POYNTER, AND E. A. COHEN. 1981. Pressure broadening of phosphine by hydrogen and helium. *J. Quant. Spectrosc. Radiat. Transfer* **26**, 197-198.

PICKETT, H. M., R. L. POYNTER, AND E. A. COHEN. 1992. Submillimeter, millimeter, and microwave spectral line catalogue. JPL Publ. 80-23, Rev. 3. JPL, Pasadena, Calif.

POYNTER, R. AND R. KAKAR. 1975. The microwave frequencies, line parameters, and spectral constants for $^{14}NH_3$. *Astrophys. J. Sup.* **29**, 87-96.

PRINN, R. G. AND J. S. LEWIS, J.S. 1975. Phosphine on Jupiter and implications for the Great Red Spot. *Science* **190**, 274-276.

PRINN, R. G., H. P. LARSON, J. J. CALDWELL, AND D. GAUTIER. 1984. Composition and chemistry of Saturn's atmosphere. In *Saturn* (T. Gehrels and M. S. Mattews, Eds.), pp. 88-149. Univ. of Arizona Press, Tucson.

RATHER, J. D. G., B. L. ULICH, AND P. A. R. ADE. 1974. Planetary brightness temperature measurements at 1.4-mm wavelength. *Icarus* **22**, 448-453.

RIDGEWAY, S. T., L. WALLACE, AND G. R. SMITH. 1976. The 800-1200 inverse centimeter absorption spectrum of Jupiter. *Astrophys. J.* **207**, 1002-1006.

ROWAN-ROBINSON, M., P. A. R. ADE, E. I. ROBSON, AND P. E. CLEGG. 1978. Millimetre observations of planets, galactic and extra-galactic sources. *Astron. Astrophys.* **62**, 249-254.

SCHNOPPER, H. W. AND R. I. THOMPSON. 1974. Fourier spectrometers. In *Methods of Experimental Physics*, **12A** (M. L. Meeks, Ed.), pp. 491-529. Academic Press, New York.

SERABYN, E., T. G. PHILLIPS, AND C. R. MASSON. 1991. Surface figure measurements of radio telescopes with a shearing interferometer. *Applied Opt.* **30**, 1227-1241.

SPILKER, T. R. 1993. New laboratory measurements on ammonia's microwave inversion spectrum, with implications for planetary atmospheres. *J. Geophys. Res.* **98**, 5539-5548.

STROBEL, D. F. 1977. NH_3 and PH_3 photochemistry in the Jovian atmosphere. *Astrophys. J. Lett.* **214**, L97-L99.

TARRAGO, G., N. LACOME, A. LEVY, G. GUELACHVILI, B. BÉZARD, AND P. DROSSART. 1992. Phosphine spectrum at 4-5 μm: Analysis and line-by-line simulation of $2\nu_2$, $\nu_2+\nu_4$, $2\nu_4$, ν_1, and ν_3 Bands. *J. Molec. Spectrosc.* **154**, 30-42.

TOKUNAGA, A. T., R. F. KNACKE, S. T. RIDGEWAY, AND L. WALLACE. 1979. High-resolution spectra of Jupiter in the 744-980 inverse centimeter spectral range. *Astrophys. J.* **232**, 603-615.

TOKUNAGA, A. T., H. L. DINERSTEIN, D. F. LESTER, AND D. M. RANK. 1980. The phosphine abundance on Saturn derived from new 10-micrometer spectra. *Icarus* **42**, 79-85.

TOKUNAGA, A. T., H. L. DINERSTEIN, D. F. LESTER, AND D. M. RANK. 1981. Erratum to: The phosphine abundance on Saturn derived from new 10-micrometer spectra. *Icarus* **48**, 540.

TOKUNAGA, A., S. BECK, T. GEBALLE, J. LACY, AND E. SERABYN. 1981. The detection of HCN on Jupiter. *Icarus* **48**, 283-289.

TOMASKO, M. G., R. A. WEST, G. S. ORTON, AND V. G. TEJFEL. 1984. Clouds and aerosols in Saturn's atmosphere. In *Saturn* (T. Gehrels and M. S. Matthews, Eds.), pp. 150-194. Univ. of Arizona Press, Tucson.

TOWNES, C. H. AND A. L. SCHAWLOW. 1975. *Microwave Spectroscopy.* Dover Publ., New York.

TRAFTON, L. M. 1965. A study of the energy balance in the atmospheres of the major planets. Ph.D. thesis. California Institute of Technology, Pasadena, Calif.

TREFFERS, R. R. 1977. Signal-to-noise ratio in Fourier spectroscopy. *Applied Opt.* **16**, 3103-3106.

ULICH, B. L., J. R. COGDELL, AND J. M. DAVIS. 1973. Planetary brightness temperature measurements at 8.6 mm and 3.1 mm wavelengths. *Icarus* **19**, 59-82.

ULICH, B. L. 1974. Absolute brightness temperature measurements at 2.1-mm wavelength. *Icarus* **21**, 254-261.

ULICH, B. L. AND R. W. HAAS. 1976. Absolute calibration of millimeter-wavelength spectral lines. *Astrophys. J. Supp.* **30**, 247-258.

ULICH, B. L. 1981. Millimeter-wavelength continuum calibration sources. *Astron. J.* **86**, 1619-1626.

VANASSE, G. A. AND H. SAKAI. 1967. In *Progress in Optics*, **VI** (E. Wolf, Ed.). North Holland Publ., Amsterdam.

WATERS, J. W. Absorption and emission by atmospheric gases. 1974. In *Methods of Experimental Physics*, **12B** (M. L. Meeks, Ed.). Academic Press, New York.

WELFORD, W. T. AND R. WINSTON. 1989. *High Collection Nonimaging Optics.* Academic Press, San Diego.

WERNER, M., G. NEUGEBAUER, J. HOUCK, AND M. HAUSER. 1978. One-millimeter brightness temperatures of the planets. *Icarus* **35**, 289-296.

WESTPHAL, J. A., W. A. BAUM, A. P. INGERSOLL, C. D. BARNETT, E. M. DE JONG, G. E. DANIELSON, AND J. CALDWELL. 1992. Hubble Space Telescope observations of the 1990 equatorial disturbance on Saturn: Images, albedos, and limb darkening. *Icarus* **100**, 485-498.

WHITCOMB, S. AND J. KEENE. 1980. Low-pass interference filters for submillimeter astronomy. *Applied Opt.* **19**, 197-198.

WINKELSTEIN, P., J. CALDWELL, S. J. KIM, M. COMBES, G. E. HUNT, AND V. MOORE. 1983. A determination of the composition of the Saturnian stratosphere using the IUE. *Icarus* **54**, 309-318.

Tables

TABLE I.: PUBLISHED VENUS BRIGHTNESS TEMPERATURES ABOVE 90 GHz.

Frequency (GHz)	T_B (K)	Reference
142.9	300 ± 21.0	Ulich 1974
150.0	294 ± 22.0	Ulich 1981*
178.6	315 ± 13.8	Rowan-Robinson *et al.* 1978
230.0	280	Clancy and Muhleman 1985
230.0	288†	Clancy and Muhleman 1991*
300.0	276 ± 14.0	Werner *et al.* 1978*

*Used in the linear calibration fit

†Provides the best model fit to 1.3 mm CO spectra; no uncertainty quoted

TABLE II.: PUBLISHED SATURN BRIGHTNESS TEMPERATURES ABOVE 90 GHz.

Frequency (GHz)	T_B (K)	HPBW	Reference
90.0	149.3 ± 4.1	78″	Ulich 1981
97.1	148.0 ± 11.0	151″	Ulich *et al.* 1973
111.1	156.0 ± 5.0	6″	Dowling *et al.* 1987
111.1	137.3 ± 4.5	ca. 6″	Grossman 1990
141.0	164.0 ± 12.0	110″	Ulich 1974
150.0	137.0 ± 11.0	52″	Ulich 1981
214.3	194.0 ± 21.0	65″	Rather *et al.* 1974
214.3	188.0 ± 11.0	74″	Courtin *et al.* 1977
214.5	143.0 ± 17.0	74″	Courtin *et al.* 1977*
227.3	140.0 ± 3.0	41″	Ulich *et al.* 1984
300.0	145.0 ± 7.0	55″	Werner *et al.* 1978
309.9	134.5 ± 3.2	33″/49″	Hildebrand *et al.* 1985†

*Rings modelled and removed

†Ring inclination < 1.5°

TABLE III.: CHI SQUARED RESIDUALS FOR VARIOUS PH_3 FITS WITH 100 MBAR CUTOFF.

PH_3 Mole Fraction (ppm)	Line Depth (K)	FWHM (GHz)	χ^2 (K^2)
1.5	44.5	7.50	2.58
2.0	46.2	8.80	1.62
2.8	47.4	10.7	1.13
3.0	47.6	11.2	1.11
3.2	47.7	11.6	1.13
4.0	48.1	13.2	1.45
5.0	48.2	14.9	2.10
Noll and Larson*	46.0	10.9	1.38

*1 ppm for 78 mbar < p < 400 mbar, 7 ppm for p > 400 mbar

TABLE IV.: PH_3 MOLE FRACTIONS FOR VARIOUS TEMPERATURE BROADENING EXPONENTS.

PH_3 Temperature Broadening Exponent	Best-fit Mole Fraction (ppm)
0.50	3.3
0.60	3.1
0.67	3.0
0.80	2.7
0.90	2.6

TABLE V.: PUBLISHED SATURNIAN PH_3 MOLE FRACTIONS* FROM INFRARED/MILLIMETER OBSERVATIONS.

PH_3 Mole Fraction (ppm)	Pressures Probed (mbar)	Wavelength of Observation (μm)	Instrument	Reference
$\gtrsim 0.8^{\dagger}$	400-700	10	CFWS	Gillet and Forrest 1974
> 0.2	400-700	10	CGS	Bregman *et al.* 1975
0.9	500-1000	3	FTS	Larson *et al.* 1980
1.6	1000-3200	5	FTS	Larson *et al.* 1980
> 0.8	400-700	10	CGS	Tokunaga *et al.* 1980, 1981
1.0	400-700	10	IRIS	Hanel *et al.* 1981
1.3 ± 0.8	400-700	10	IRIS	Courtin *et al.* 1984
$0.6^{+0.6}_{-0.3}$	< 100	100	CGS	Haas *et al.* 1985, 1986
$5.0^{\ddagger}$	4000	5	FTS	Bézard *et al.* 1987
3.0	1000-3200	5	FTS	Noll 1987
$7.0^{+3.0}_{-2.0}$	> 400	5	FTS	Noll and Larson 1990
3.0 ± 1.0	100-1000	1100	FTS	this paper

*concentrations given relative to the hydrogen abundance have been converted assuming an H_2 mole fraction of 0.963

†tentative detection

‡this best current value (Bézard, pers. comm. 1994) is slightly higher than the published 4.0 ppm

CFWS: cooled filter-wheel spectrometer, CGS: cooled grating spectrometer, FTS: Fourier transform spectrometer, IRIS: Voyager infrared interferometer spectrometer (an FTS)

Figure Captions

Fig. 1.: CSO zenith atmospheric transmission for 1 mm precipitable H_2O, generated using the program AT (E. Grossman 1989). Deep absorptions are caused by H_2O and O_2; the many small absorption features are primarily due to O_3, although a few $O^{18}O$ lines are also present.

Fig. 2: Responsivity of the CSO bolometer detector with the CSO's "1300 μm" wire-mesh filter. The thin solid curve is the measured responsivity at full resolution; the thick solid curve is the responsivity measured at lower resolution. At full resolution, interference ripples produced by multiple reflections inside the Winston cone are quite prominent.

Fig. 3: Corrected antenna temperatures, in units of T_A^*, for (a) Saturn (with a total of 48 scans "on" source, giving an "on" integration time of 35 minutes), (b) Venus (40 scans; 29 minutes), and (c) Jupiter (56 scans; 41 minutes). In Fig. 3a, the inset indicates the observing geometry for Saturn on July 11, 1993. In Fig. 3b, the inset shows the ratio of the Venus spectrum to the Saturn spectrum near the CO line.

Fig. 4: Solid line: calibrated Saturn brightness temperature spectrum. Dashed line: Lorentzian best fit with linear baseline. The region near 230 GHz has been blanked to suppress the narrow CO absorption line observed in Venus (the calibration source), preventing it from appearing spuriously in the Saturn spectrum. The central frequencies of several lines with rotational transitions in the passband are marked.

Fig. 5: Saturn models for stratospheric HCN (solid lines) and the same convolved to our 205 MHz instrumental resolution (dashed lines). Thin lines are 2 ppb HCN; thick lines are 4 ppb HCN. PH_3 is taken to have a mole fraction of 3.0 ppm.

Fig. 6: Model PH_3 central line cores for various atmospheric cutoff pressures. The line cores have been convolved to our instrumental resolution of 205 MHz.

Fig. 7: Saturn models for various atmospheric cutoff pressures near and below the tropopause. In the troposphere, the line depth increases as the cutoff pressure is moved to higher altitudes (cooler temperatures).

Fig. 8: Saturn spectrum calibrated in units of brightness temperature, with superimposed model predictions for 1.5, 3.0, and 5.0 ppm PH_3. The region immediately surrounding 230 GHz has been blanked to remove the effects of the narrow CO line observed in Venus.

Fig. 9: Saturn weighting functions for (a) 210.9 GHz ($\Delta\nu = 10\alpha$), (b) 258.5 GHz ($\Delta\nu = 1.5\alpha$), (c) 261.3 GHz ($\Delta\nu = \alpha$), and (d) 264.1 GHz ($\Delta\nu = 0.5\alpha$), where α is the Lorentzian HWHM and $\Delta\nu$ is the frequency offset from the PH_3 line center. The discontinuity evident in the PH_3 weighting function slope at $p_c = 100$ mbar results from our assumed PH_3 cutoff level.

Fig. 10: Dotted line: data from Fig. 4. Solid line: model spectrum for the mixing ratio given by Noll and Larson 1990 (1 ppm for 78 mbar $0 < p < 400$ mbar, 7 ppm for $p > 400$ mbar). Dashed line: model spectrum for a constant PH_3 mixing ratio of 3.0 ppm for $p > 100$ mbar (central curve from Fig. 8).

Fig. 11: Adiabatically extrapolated pressure-temperature profile from Lindal (1992) used in the Saturn atmospheric model.

Figure 1

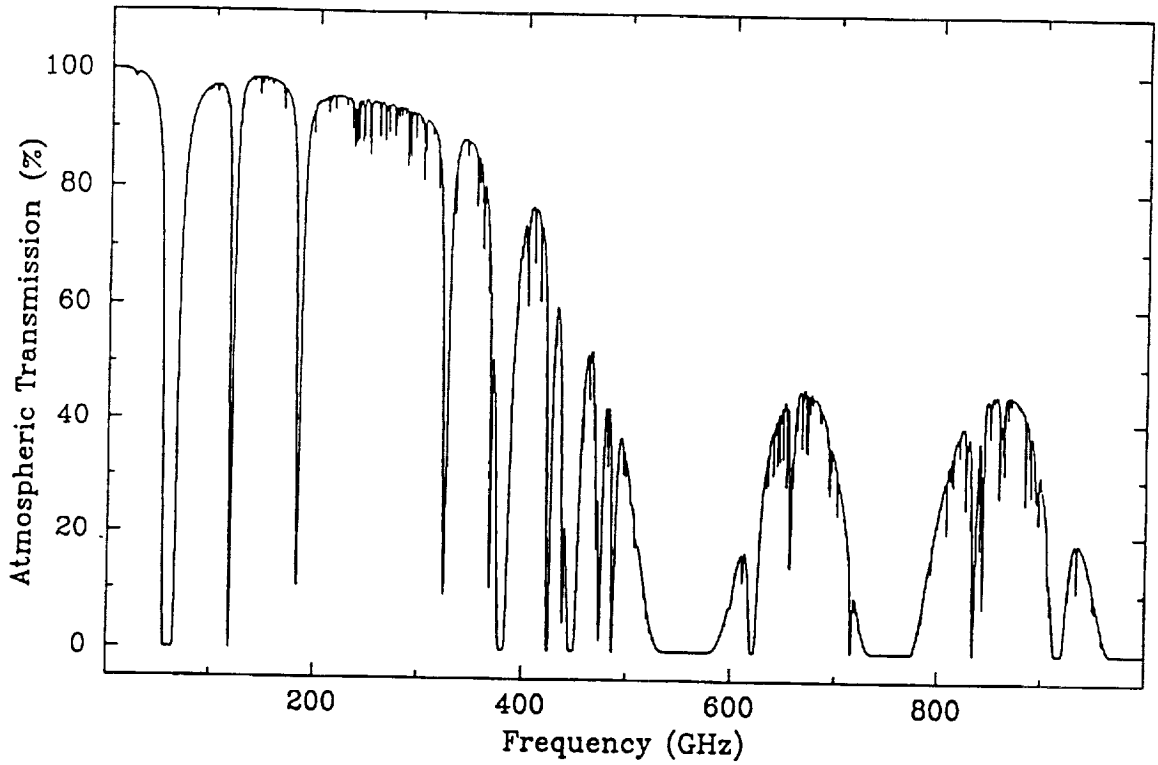

Figure 2

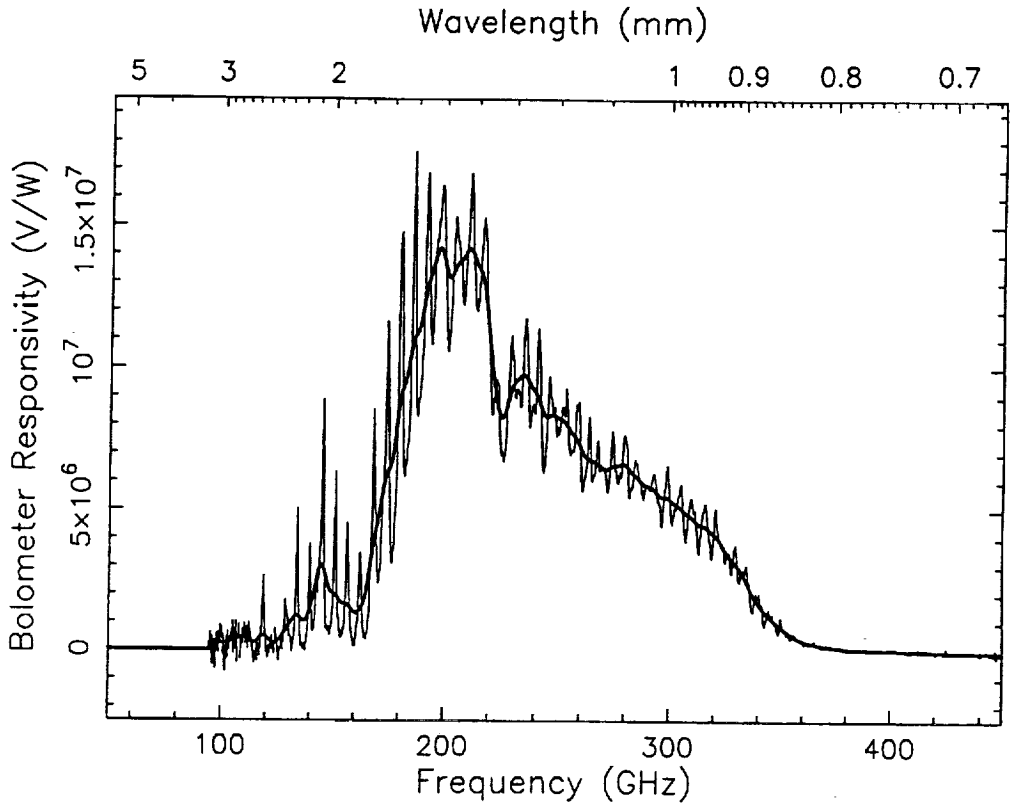

Figure 3a

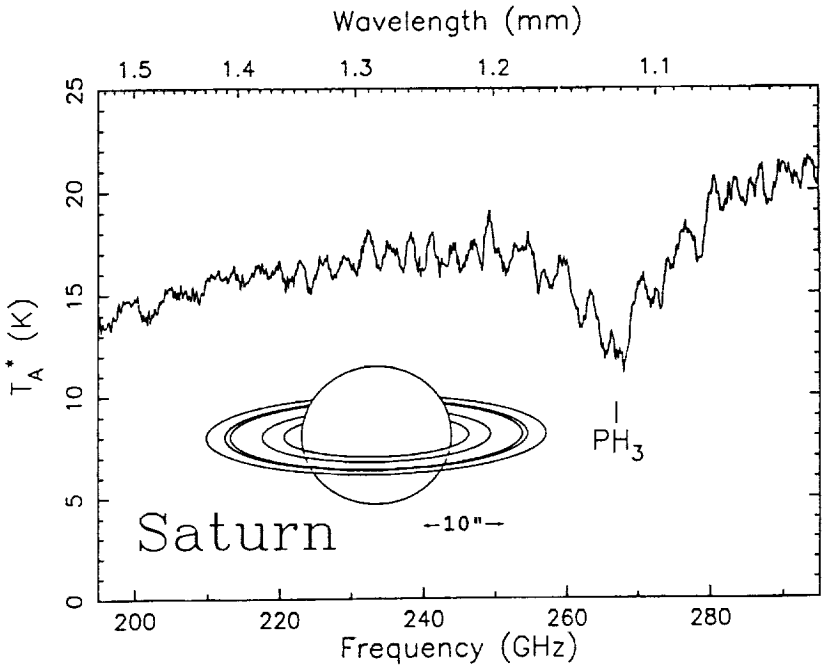

Figure 3b

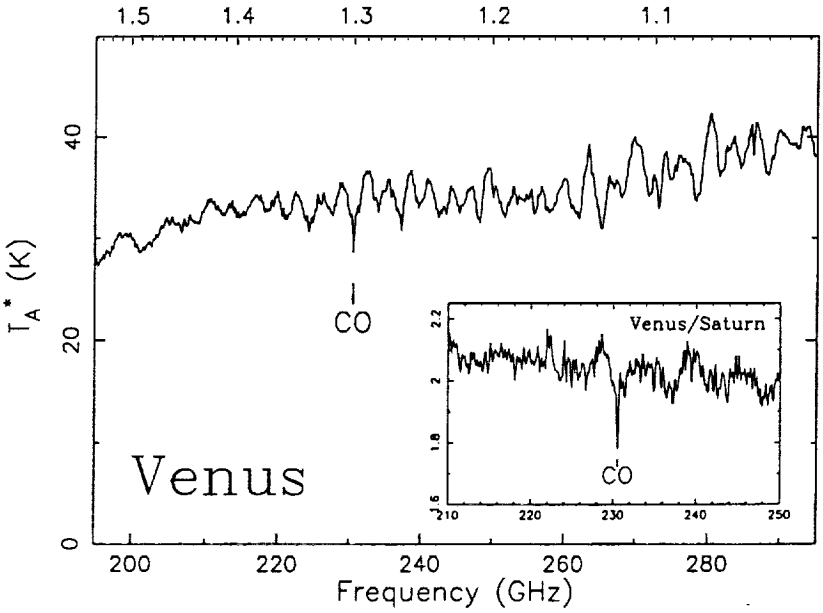

Figure 3c

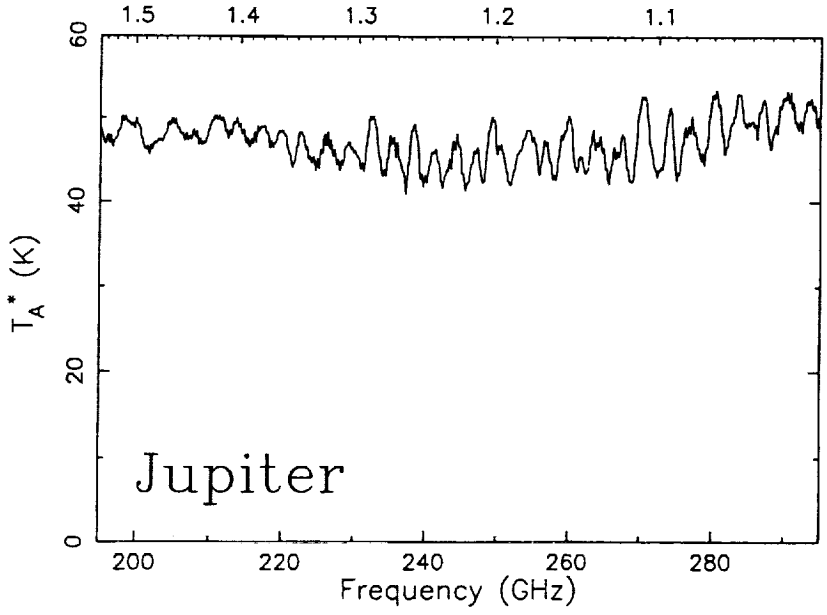

Figure 4

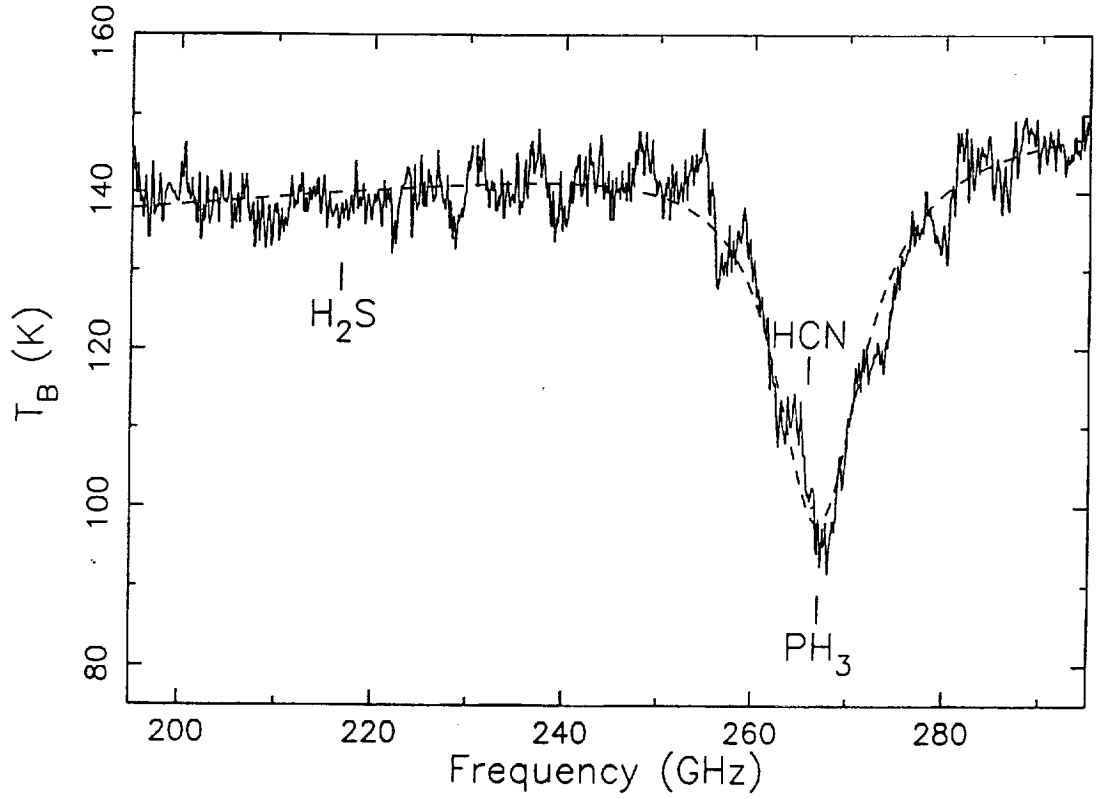

Figure 5

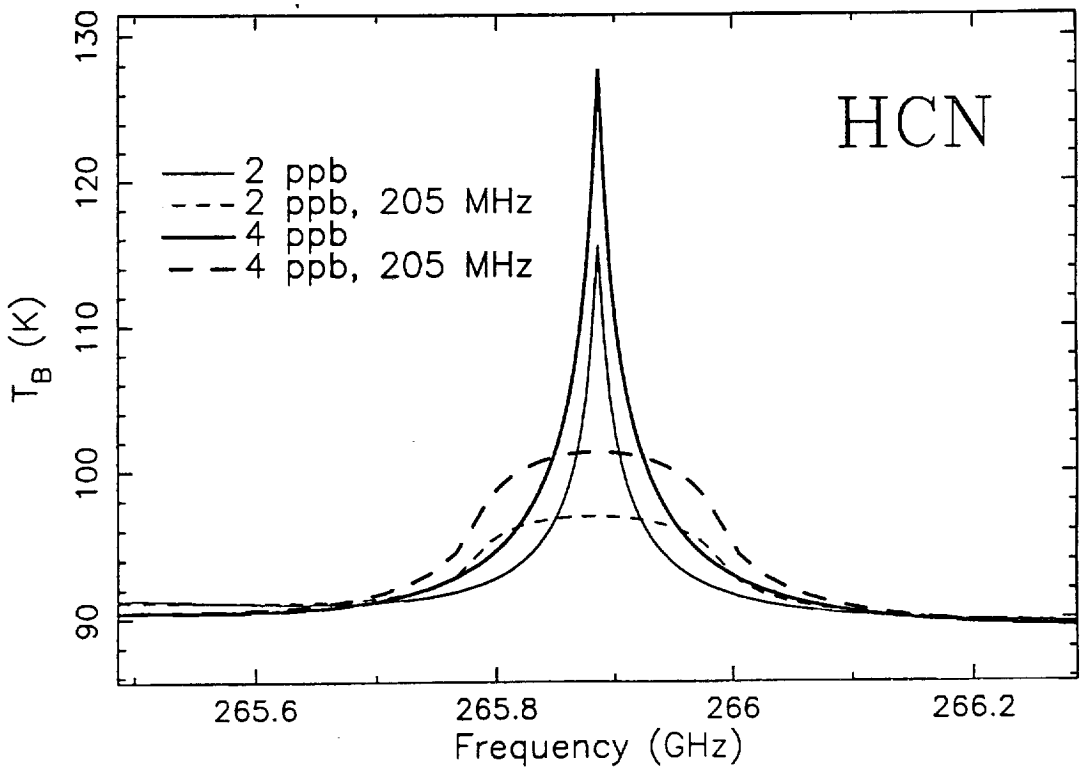

Figure 6

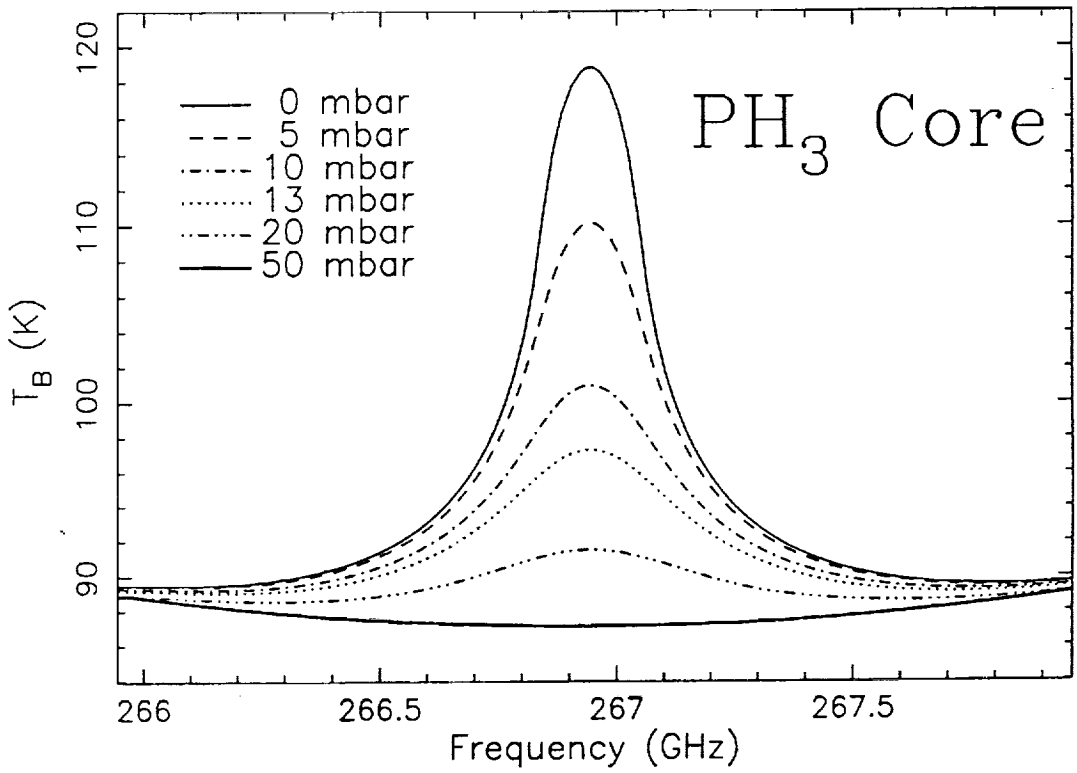

Figure 7

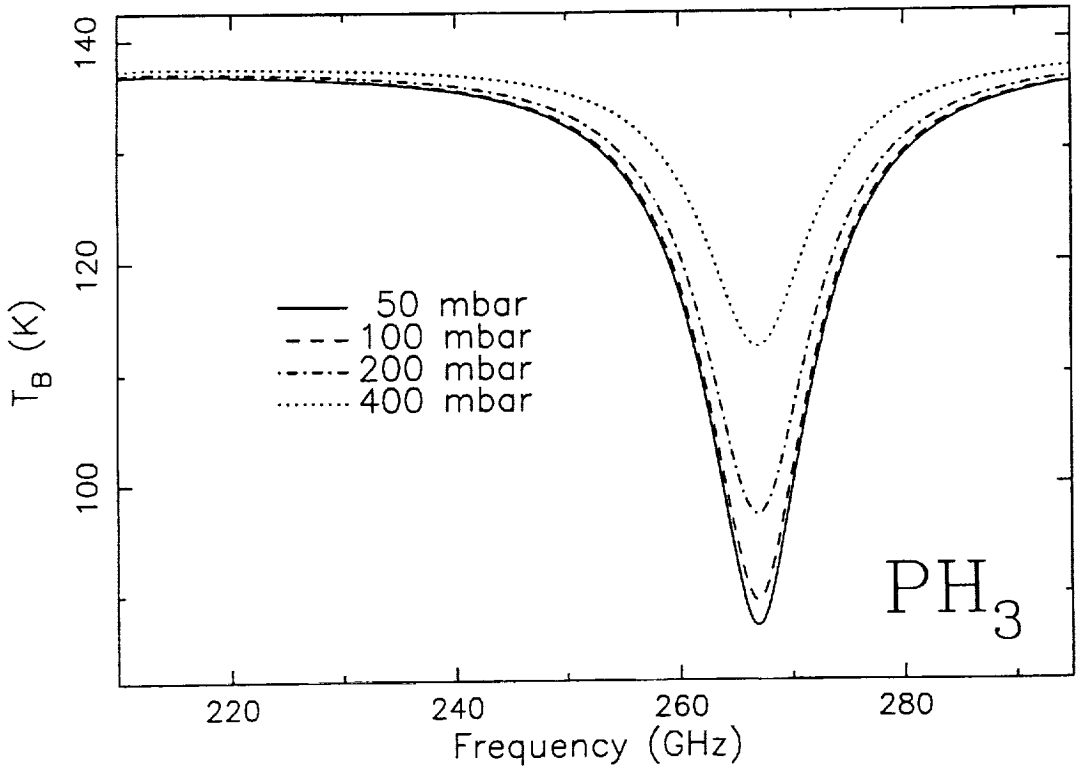

Figure 8

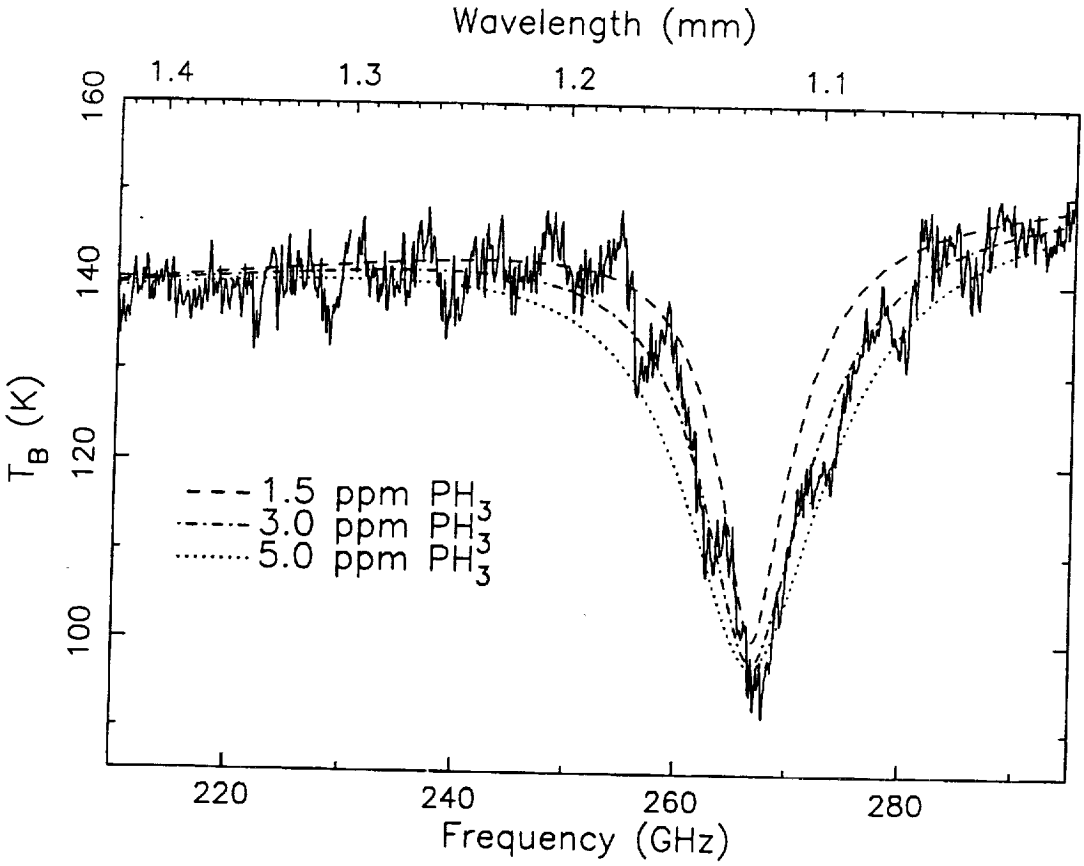
Wavelength (mm)
1.4
1.3
1.2
1.1
160
140
120
100
T_B (K)
1.5 ppm PH_3
3.0 ppm PH_3
5.0 ppm PH_3
220
240
260
280
Frequency (GHz)

Figures 9a-d

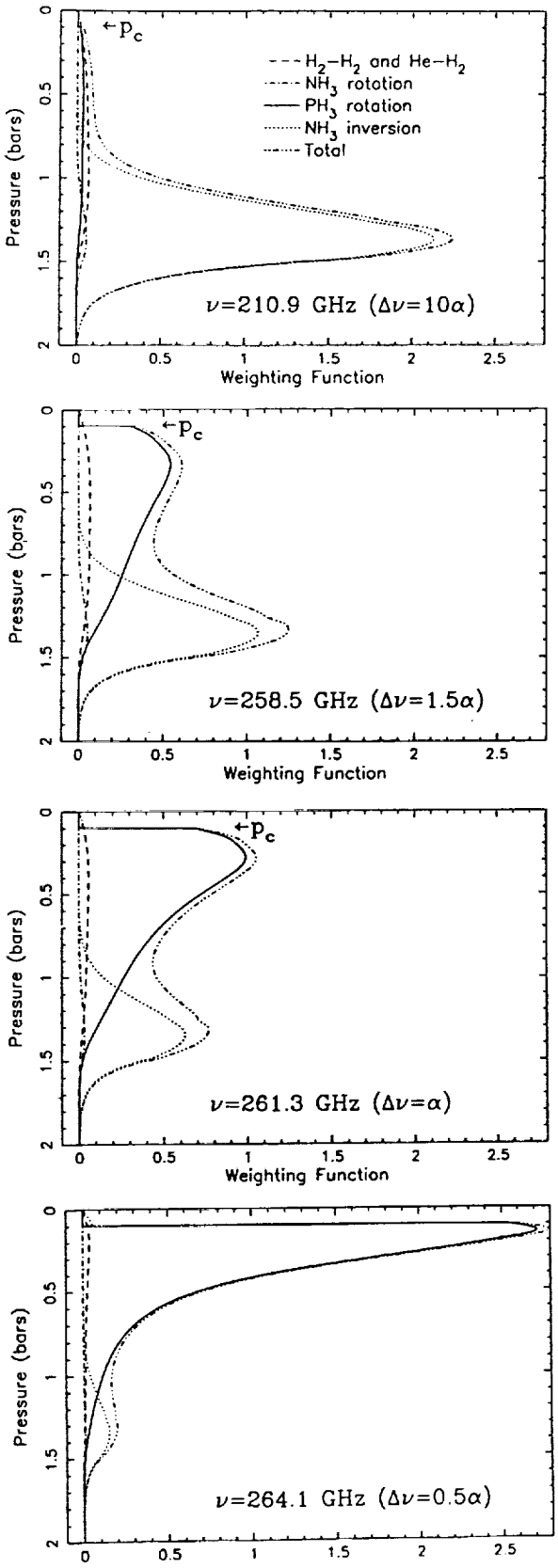
←Pc
H2–H2 and He–H2
NH3 rotation
PH3 rotation
NH3 inversion
Total
Pressure (bars)
Weighting Function
ν=210.9 GHz (Δν=10α)
←Pc
Pressure (bars)
Weighting Function
ν=258.5 GHz (Δν=1.5α)
←Pc
Pressure (bars)
Weighting Function
ν=261.3 GHz (Δν=α)
Pressure (bars)
ν=264.1 GHz (Δν=0.5α)

Figure 10

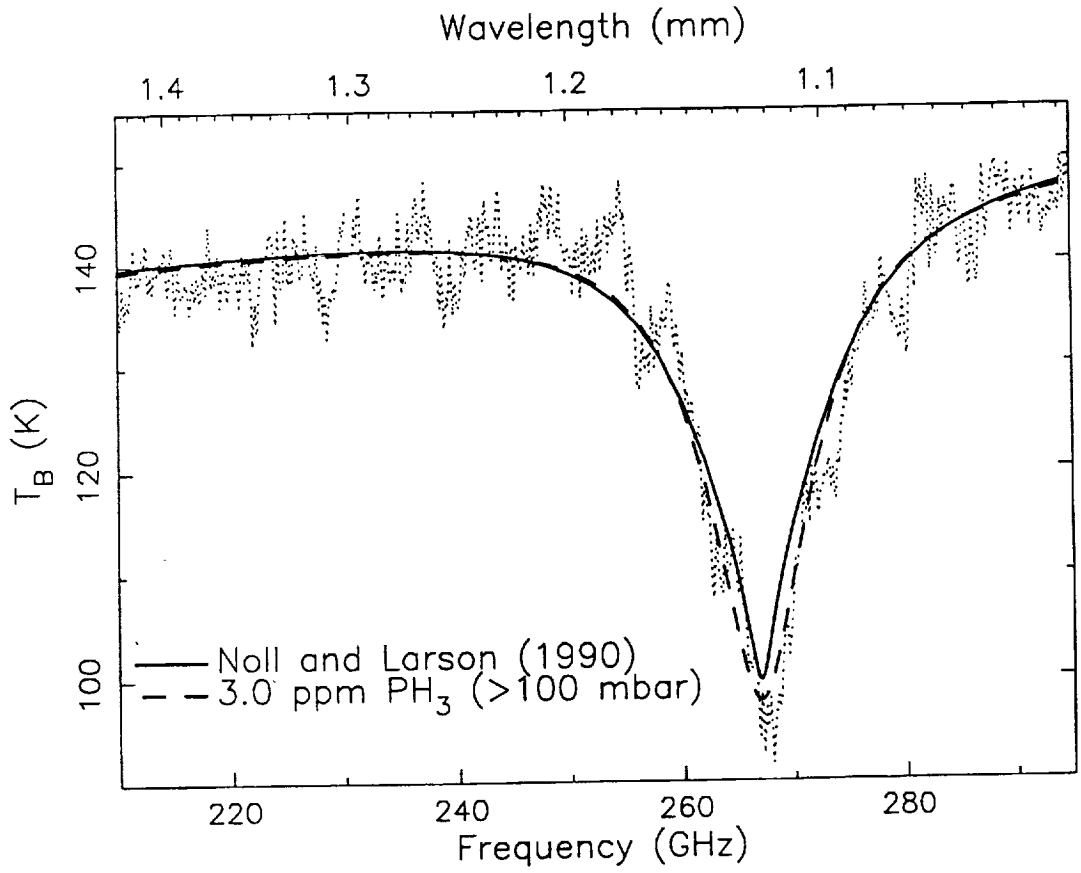

Figure 11